Journal of Engg. Research Vol. 7 No. (2) June 2019 pp. 45-65

A numerical model to simulate fracture network induced by hydraulic fracturing for 3D shale gas reservoir with geo-stress interference

Qiang Wang*, Yongquan Hu , Jinzhou Zhao and Lan Ren

State Key Laboratory of Oil-Gas Reservoir Geology & Exploitation, Southwest Petroleum University, Chengdu 610500, China
**Corresponding Author: 201521000196@stu.swpu.edu.cn*

ABSTRACT

In the two-dimensional simulated reservoir volume (SRV) model, the position of natural fractures is determined only by the approaching angle, and it is only required to consider the influence of horizontal principal stress in its failure criterion. In the three-dimensional shale reservoir, the position of natural fracture needs to be determined by the dip angle and approaching angle while considering the influence of vertical and horizontal principal stress in its failure criterion. In addition, the simultaneous opening of several hydraulic cracks will lead to the change of geo-stress, thus causing the change of the conditions of the natural fracture and shear failure by the induced tress. In order to analyze the generation of three-dimensional fracture network, this paper establishes a mathematical model based on elastic mechanics, three-dimensional rock failure criterion, full permeability tensor, and material conservation equation. Firstly, the finite element method model of geological stress caused by fracturing is established based on the crack propagation model, and the finite difference method module based on three-dimensional fluid diffusion control equation and full permeability tensor is used to solve the reservoir pressure distribution. Then, the three-dimensional rock tensile and shear failure criteria are used to determine whether any grid units are destroyed. Once a grid has occurred in any form of rock failure criterion, the permeability of the corresponding grid unit will also change due to the change of natural fracture opening. Finally, the stimulated reservoir volume is represented by the region of increased permeability. This paper presents the sensitivity analysis of the multi-factor after using the micro-seismic data to validate the numerical model, including the influence of injected fluid volume, natural fracture approaching Angle, dip Angle and horizontal principal stress difference on the size of SRV (shape, size, border width, length, etc.). Results show that, compared to without the induced stress, the tensile failure volume decreases and the shear failure volume increases, while the total SRV increases due to the induced stress. When the vertical principal stress in the three-principal stress is maximum, the length of the SRV increases with the increase of natural fracture approaching angle, dip angle and horizontal principal stress difference, but its width decreases. Its width and length increase at the same time only with the increase volume of injected fluid; the size of SRV increases with the increase of the injection fluid volume and the natural fracture dip, but decreases with the increase of the natural fracture approaching angle and horizontal principal stress difference.

Keywords: Shale gas; SRV; Tensile failure; Shear failure; Total permeability tensor; Stress interference.

INTRODUCTION

The permeability of shale gas reservoir matrix is quite low, but the natural fractures are very developed. Natural fractures can be activated, and a complex network can be formed by hydraulic fracturing, which can cause shear or tensile failure of natural fractures (Mayerhofer et al., 2010; Hu et al., 2016). But current research mainly adopts two-dimensional model to predict stimulated volume and study the generating mechanism of the fracture network. The position of natural fractures in the two-dimensional model is only determined by the azimuth (approaching) angle,

without considering the influence of dip angle. The failure criterion in the two-dimensional model also considers the influence of horizontal principal stress and ignores the effect of vertical principal stress. Therefore, the two-dimensional model used to predict the stimulated volume is different from the actual situation. In order to obtain more accurate production performance evaluation and optimize hydraulic fracturing parameters in shale reservoir, a stimulated reservoir volume (SRV) prediction model considering stress interference, dip angle, three-dimensional rock failure criterion, full permeability tensor, 3d diffusion, etc. needs to be established.

The microseismic data can prove that, in the process of hydraulic fracturing, the fracture network rather than the single plane crack is generated in the shale reservoir(Cipolla, 2009;Yu and Aguilera, 2012). So the hydraulic fracturing technique has great influence on the transforming volume of the shale reservoir. The effect is that hydraulic fracturing technology promotes the generation of fracture network and establishes the high-speed channel of shale gas flow, which builds the foundation for the later development of shale gas. However, there is no accurate understanding of the mechanism of fracture network. In the early stage of the study on the formation mechanism of the fracture network, the length of hydraulic fracture is generally considered as constant. Some analytic models were proposed to predict the shear failure of natural fractures (Palmer, 2007, 2009 & 2013; Warpinski et al., 2001). They believed that shear failure would activate natural fractures. Ge and Ghassemi (2012) proposed an analytical solution based on the Mor-Coulomb failure criterion to predict the shear failure of natural fractures. Wang et al. (2016) established a model of coupling fluid flow, stress and rock failure to evaluate the impact of shear failure in shale gas reservoir and conducted parameter sensitivity analysis. However, some scholars believe that, in the process of hydraulic fracturing, natural fractures will not only cause shear failure, but also will have a tensile failure. Therefore, some people successively proposed some models considering natural fracture tensile and shear failure models (Ren, 2015 & 2016; Nassir et al., 2012 & 2014; Ghassemi, 2013; Maulianda et al., 2014; Shahid et al., 2015). In these models, geological stress, reservoir pore pressure, rock deformation, and other factors also were considered. For the simulation of complex fracture network, the biggest difficulty lies in the treatment of natural fractures. The main models used today are orthogonal natural fracture model (Xu, 2009 & 2010), Pseudo-3D (Weng et al., 2011), and discrete natural fracture model (Zou et al., 2016). However, in the orthogonal natural fracture model the tensile and shear failure of natural fractures are not considered, and the effect of stress has not been taken into account in the Pseudo-3D model. Then, the computation time of discrete model is quite long, and each crack needs to be separated separately. Therefore, a new 3D model is built to overcome these shortcomings.

As shown in Fig. 1a, for engineering application, a single segment example with three clusters of fractures in a horizontal fracturing well is used for research. During fluid injection, the increase of reservoir pore pressure produces a destructive region called SRV region, as shown in Fig. 1b. In order to describe the growth process of SRV, a SRV prediction model based on stress interference, 3D permeability tensor, and fluid material balance was proposed. In this model, the actual distribution of natural fractures is reduced to a spatial distribution conjugate fracture. Since the distribution and state of complex natural fractures need not be described, this model has more efficient computational efficiency than discrete fracture method. This model can provide a more efficient and accurate tool for hydraulic fracturing operation design in shale gas reservoir.

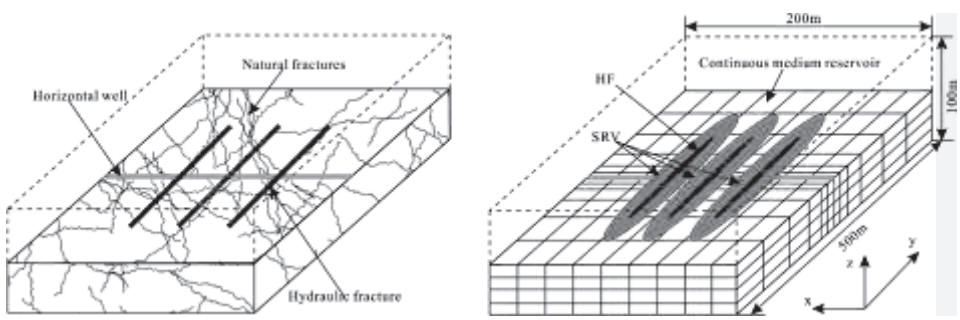

(a) (b)

Fig. 1. The schematic diagram of hydraulic fracturing (a) and simplified shale fracturing diagram (b) in shale reservoir.

Mathematical model

The hydraulic crack extension model

The fluid flow in the hydraulic main fracture is generally assumed to flow between two plates. The average flow velocity of fluid can be obtained from the Navier-Stokes equation, and its general form is (Zimmerman et al., 1991)

$$v_s = -\frac{W^2}{12\mu}\frac{\partial p_f}{\partial x} \tag{1}$$

where v_s is fluid flow velocity in hydraulic fracture, m/s; W is the crack width, m; p_f is the fluid pressure inside the fracture, MPa; μ is the fluid viscosity in the fracture, mPa.s.

According to the principle of mass conservation, the amount of injected fluid is equal to the sum of the fluid in the fracture and the fluid of filtration into the reservoir:

$$\frac{\partial W}{\partial t} + \nabla \cdot (v_s W) + W Q_s = 0 \tag{2}$$

where Q_S is the source sink item, 1/s.

Substituting equation (1) into equation (2), the following equation can be obtained:

$$W\left(Q_{inje} + Q_{leak}\right) + \frac{\partial W}{\partial t} = \nabla \cdot \left(\frac{W^3}{12\mu}\nabla p_f\right) \tag{3}$$

where Q_{inje} is the source of injection, 1/s; Q_{leak} is the source of filtration, 1/s; t represents fracturing time, s.

In the process of hydraulic fracturing, natural fractures near hydraulic crack are first affected by filtration into the reservoir fluid, so near the hydraulic fracture permeability and pore fluid pressure in the first begin to change. These two changes have a great influence on fluid filtration in hydraulic fracture. Considering that fracturing fluid filtration is controlled by pressure and permeability between hydraulic fractures and reservoir, the following filtration model is adopted:

$$Q_{leak} = \frac{K_m S_s}{\mu} f\left(p_f - p_p\right) \tag{4}$$

where K_m is the matrix permeability after transformation, μm^2; S_S represents filtration area, m^2; f is the permeability coefficient, 1/m; p_p is reservoir pore pressure, MPa.

The geologic stress model

In the staged fracturing, type I rock failure occurs with the affection of fluid pressure on the cracks (Zhou et al., 2015), and the hydraulic cracks propagate along the direction of the maximum principal stress, as shown in Fig2. As introduced in Zhou and Hou (2013), an extra strain increment induced by pressure change in the fracture was added in the total strain increment to describe the discontinuous behavior of fracture. Due to the extra strain, the distribution and size of geo-stress in reservoir will be changed. It is shown that the tensile and shear failure of natural fractures are greatly influenced by the change of geological stress (Ren L et al., 2017). The equilibrium equation of the volume field and the Hooke's law of linear elastic media can be written as the following tensor form:

$$\nabla \cdot S + b = 0 \tag{5}$$

$$S = C : E(U) \tag{6}$$

where C is the elastic constant tensor; S, U are the stress field and the displacement field, respectively; b represents the body force tensor; $E(U)$: represents the double dot product of two tensors; $E(U)$ is the strain tensor associated with the displacement.

$$E(U)=\frac{1}{2}\left(\nabla U+(\nabla U)^{T}\right) \tag{7}$$

The displacement of the outer boundary of the model is given by a given function $G(x,y)$:

$$U\big|_{\Gamma}=G \tag{8}$$

Crack width can be defined as

$$W=\left(U^{+}-U^{-}\right)\cdot n \tag{9}$$

where n is the unit normal vector on the crack surface U^{+}; U^{-}, are the displacements of the upper and lower wall of the fracture, respectively, m.

The stress boundary and displacement boundary of elastic equation should be satisfied:

$$\begin{cases} S\cdot n=F & \Gamma_{F} \\ S\cdot n^{-}=-S\cdot n^{+}=-p_{net}\cdot n^{+}=p_{net}\cdot n^{-} & \Gamma_{f} \\ U=U_{o} & \Gamma_{U} \end{cases} \tag{10}$$

where $\Gamma\big|_{F}$、$\Gamma\big|_{f}$、$\Gamma\big|_{U}$ represent the external force boundary, fracture boundary, and displacement boundary of the model, respectively.

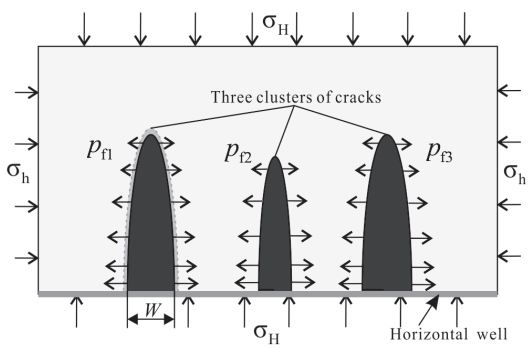

Fig. 2. Schematic diagram of geological stress disturbance.

Natural fracture failure criterion

The shale reservoir is a very developed reservoir of natural fractures, but its permeability is very low. When the fluid is injected, the pore pressure of the reservoir increases rapidly, which may cause the opening of natural fractures in the reservoir or the tensile and shear failure. In the process of fracturing, the pore pressure of the reservoir near the hydraulic fracture is greater than the normal stress on the natural fracture surface, and the natural fracture will produce a certain degree of opening, which will increase the crack permeability rapidly.

$$p_{p}\geq\sigma_{n} \tag{11}$$

where σ_n represents the normal stress on the natural fracture surface, MPa.

As the fluid pressure of natural fractures continues to increase, its value is more than normal stress on the surface of the natural fracture and tensile strength of rocks. Then, natural fracture tensile failure will occur. According to the rule of Warpinski, its condition is (Warpinski et al., 1987)

$$p_{p}\geq\sigma_{n}+T_{0} \tag{12}$$

whereT_0 is the tensile strength of the reservoir rock, MPa.

The discriminant of natural fracture shear failure is

$$\sigma_\tau > \tau_0 + \lambda\left(\sigma_n - p_p\right) \tag{13}$$

where σ_τ is the shear stress of the natural fracture wall, MPa;τ_0 represents the natural fracture cohesion, MPa; λ is the natural fracture friction coefficient, dimensionless.

Equations (12) and (13) are the main basis for determining the tensile failure and shear failure. In the 2D plane model, the natural fractures are considered as vertical fractures, ignoring the effect of vertical principal stress. In the actual shale reservoir, the spatial distribution of natural fractures is very directional, but not all vertical fractures. In order to apply the rock failure criterion to the three-dimensional SRV calculation, this paper deduces the normal stress and shear stress on the natural fracture surface at any space position (Ren et al., 2015; Ren et al., 2017).

The unit normal vector of natural fracture is

$$\overline{n} = n_i e_i = \begin{bmatrix} n_x & n_y & n_z \end{bmatrix} \tag{14}$$

among them

$$n_x = \sin\phi\cos\alpha \tag{15}$$

$$n_y = \sin\phi\sin\alpha \tag{16}$$

$$n_z = \cos\phi \tag{17}$$

where $\overline{n}$ represents natural fracture unit normal vector, dimensionless; n_i represents the unit normal vector component of natural fracture, dimensionless, $i \in \{x, y, z\}$; α is the angle between the natural fracture and the horizontal maximum principal stress direction (approaching angle), $^\circ$;ϕ is the angle between the natural fractures and the horizontal plane (dip angle), °; the approaching angle and dip angle of natural fractures are shown in Fig. 3.

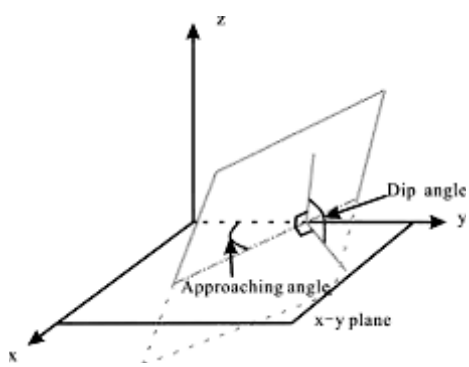

Fig. 3. The spatial distribution of natural fractures.

At this point, the force acting on the natural fracture surface is

$$\overline{F} = \overline{\overline{\sigma}}\,\overline{n} = \sigma_{ij} e_i e_j n_k e_k = \sigma_{ij} n_k e_i \delta_{ij} = \sigma_{ij} n_j e_i \tag{18}$$

where $\overline{\overline{n}}$ represents the second order symmetric tensor of in situ stress, MPa; σ_{ii} represents the stress tensor component, MPa; e_i 、 e_j 、 e_k, respectively, represents the orthonormal basis vectors; $\overrightarrow{F}$ represents the force exerted on the wall surface of natural fractures, MPa; δ_{ij} is the Kronecker symbol; i, j, k respectively, are the coordinate indices and represent x, y and z.

The force is decomposed into the normal direction of the natural fracture surface, which is the normal stress for the fracture wall surface:

$$\sigma_n = \vec{F}\vec{n} = n_k e_k \sigma_{ij} n_j e_i = n_k \sigma_{ij} n_j \delta_{ij} = n_i \sigma_{ij} n_j \tag{19}$$

According to the principle of force synthesis, the shear stress value of the force along the natural fracture wall is obtained:

$$\sigma_\tau = \sqrt{\vec{F}\vec{F} - \sigma_n^2} = \sqrt{\sigma_{ij} n_j e_i \sigma_{ij} n_j e_i - \sigma_n^2} = \sqrt{\sigma_{ij} n_j \sigma_{ij} n_j - \sigma_n^2} \tag{20}$$

The normal stress and shear stress of natural fracture wall can be calculated through equations (19) and (20), then plugging in equation (5) can determine whether the cracks are open, and plugging in equations (12) and (13) can distinguish whether it is the natural fracture tensile or shear failure.

The fracture deformation and reservoir permeability model

In the shale reservoir, the permeability of the matrix is quite low, but the permeability of the matrix will be greatly increased due to the increase of natural fracture opening caused by the tensile and shear failure of natural fractures (Fredd et al., 2001; Zhang et al., 2013). When the tensile failure of natural fracture occurs, the fracture surface produces a normal strain, and its value is related to the fluid pressure in the natural fracture, the normal stress on the fracture surface, and the normal stiffness of the crack. This relationship can be expressed as follows (Guo et al., 2014a; Guo et al., 2014b):

$$w_n = \frac{p_p - \sigma_n}{K_n} \tag{21}$$

where K_n is the natural fracture normal stiffness, MPa/m; W_n is the normal opening degree of natural fractures, m.

Shear slip effect occurs when shear failure occurs in natural fractures. The natural crack opening caused by shear slip can be expressed by the following equation (Hossain et al., 2002):

$$w_s = \frac{\sigma_\tau}{K_s} \tan \varphi_d \tag{22}$$

where W_S represents the natural crack opening caused by shear slip, m; K_S is shear stiffness for natural fractures, MPa/m; φ_d is the shear expansion angle, °.

Based on the above analysis, it can be seen from the linear elasticity theory that the total opening degree of natural fractures can be expressed as follows:

$$w_a = w_0 + w_n + w_s = w_0 + \frac{p_p - \sigma_n}{K_n} + \frac{\tau_n}{K_s} \tan \varphi_d \tag{23}$$

where w_a is the total opening degree of natural fractures, m; w_0 is the initial opening of natural fractures, m.

For natural fracture zones where only shear failure occurs, the total opening degree is the sum of initial opening and shear opening:

$$w_a = w_0 + w_s = w_0 + \frac{\tau_n}{K_s} \tan \varphi_d \tag{24}$$

According to the cubic law, the equivalent volume permeability of natural fractures in the shale reservoir can be obtained:

$$K_f = \frac{w_a^3}{12 S_f} \tag{25}$$

where K_f is the equivalent permeability of natural fractures in the grid node, μm^2; S_f is the spacing of natural fractures, m.

The natural fractures in shale reservoirs is random distribution, so natural fracture position must have a certain

angle with the global coordinate system. Therefore, the natural fracture permeability in the x_1、 y_1、 z_1 direction of the local coordinate system needs to be transformed into the permeability in x_g、 y_g、 z_g direction of the global coordinate system. Therefore, by rotating the local coordinate system, the permeability components of each direction in the global coordinate system can be obtained (Fanchi et al., 2008). The natural fracture permeability tensor in global coordinate system can be expressed as

$$\underline{\underline{K}} = \overline{D}\begin{pmatrix} K_x \\ K_y \\ K_z \end{pmatrix} = \begin{pmatrix} K_{xx} & K_{xy} & K_{xz} \\ K_{yx} & K_{yy} & K_{yz} \\ K_{zx} & K_{zy} & K_{zz} \end{pmatrix} \tag{26}$$

$$\overline{D} = \begin{bmatrix} \dfrac{\cos\omega\cos\xi}{\left(\cos^2\omega+\cos^2\xi\right)^{1/2}} & \dfrac{\cos\xi\cos\psi}{\left(\cos^2\omega+\cos^2\xi\right)^{1/2}} & -\left(\cos^2\omega+\cos^2\xi\right)^{1/2} \\ \dfrac{\cos\xi}{\left(\cos^2\omega+\cos^2\xi\right)^{1/2}} & \dfrac{\cos\omega}{\left(\cos^2\omega+\cos^2\xi\right)^{1/2}} & 0 \\ \cos\omega & \cos\xi & \cos\psi \end{bmatrix} \tag{27}$$

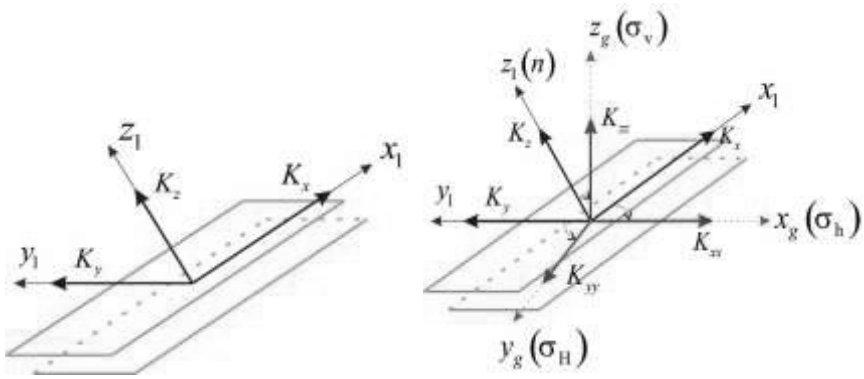

(a) (b)

Fig. 4. The schematic diagram of local coordinates and global coordinate transformation.

where $\underline{\underline{K}}$ is the permeability tensor of natural fractures, μm^2; $\overline{D}$ is the coordinate rotation matrix; K_x、 K_y、 K_z are the permeability of the x_1、 y_1、 z_1 direction in the local coordinate system μm^2; K_{xx}、 K_{xy}、 K_{yy}、 K_{zy}、 K_{zz}、 K_{xz} are the permeability components in the global coordinate system; ω、 ξ、 ψ are the angles between z_1-axis and x_g-axis, y_g-axis, z_g-axis, respectively; In Fig. 4, σ_v、 σ_H、 σ_h are the vertical principal stress, horizontal maximum principal stress, and horizontal minimum principal stress, respectively.

The fluid seepage model

In the fractured reservoir, the continuous double porosity model and the discrete fracture model are widely used in the seepage calculation of shale reservoir. Although the discrete fracture model can accurately describe the flow process of fluid in natural fractures, the computational efficiency of the shale reservoir with extremely developed natural fractures is too low. In order to simplify the model, an equivalent single pore model is used to simulate the flow process of the total fluid flow in the fractured shale reservoir (Nassir et al., 2012 & 2014). Therefore, the material balance equation of single-phase fluid in this three-dimensional model can be expressed as

$$\frac{\partial}{\partial x}\left(\frac{K_{xx}}{\mu B}\left(\frac{\partial p_p}{\partial x}\right)\right)+\frac{\partial}{\partial x}\left(\frac{K_{xy}}{\mu B}\left(\frac{\partial p_p}{\partial y}\right)\right)+\frac{\partial}{\partial x}\left(\frac{K_{xz}}{\mu B}\left(\frac{\partial p_p}{\partial z}\right)\right)+\frac{\partial}{\partial y}\left(\frac{K_{yx}}{\mu B}\left(\frac{\partial p_p}{\partial x}\right)\right)+\frac{\partial}{\partial y}\left(\frac{K_{yy}}{\mu B}\left(\frac{\partial p_p}{\partial y}\right)\right)$$
$$+\frac{\partial}{\partial y}\left(\frac{K_{yz}}{\mu B}\left(\frac{\partial p_p}{\partial z}\right)\right)+\frac{\partial}{\partial z}\left(\frac{K_{zx}}{\mu B}\left(\frac{\partial p_p}{\partial x}\right)\right)+\frac{\partial}{\partial z}\left(\frac{K_{zy}}{\mu B}\left(\frac{\partial p_p}{\partial y}\right)\right)+\frac{\partial}{\partial z}\left(\frac{K_{zz}}{\mu B}\left(\frac{\partial p_p}{\partial z}\right)\right)+q=\frac{\partial}{\partial t}\left(\frac{\phi}{B}\right) \quad (28)$$

where ϕ is reservoir porosity, dimensionless; q represents the injection fluid volume per unit reservoir volume and time, s^{-1}; μ is fluid viscosity, $mPa \cdot s$; B is fracturing fluid volume coefficient, dimensionless.

For compressible fluid, the fluid volume coefficient can be defined as

$$B=\frac{B_0}{\left[1+C_1\left(p_p-p_i\right)\right]} \quad (29)$$

where C_1 is the fluid compressibility factor, MPa^{-1}; B_0 is the fluid volume coefficient under reference pressure, dimensionless ; p_i is the initial reservoir pore pressure, MPa.

The relationship between rock porosity and reservoir pressure can be expressed as

$$\phi=\phi_0\left[1+C_r\left(p_p-p_i\right)\right] \quad (30)$$

where ϕ_0 is the initial reservoir porosity, dimensionless; C_r represents the compressibility of the rock, MPa^{-1}.

Boundary condition:

$$\left.\frac{\partial p_p}{\partial x}\right|_{x=0}=0,\ \left.\frac{\partial p_p}{\partial y}\right|_{y=0}=0 \quad (31)$$

$$\left.\frac{\partial p_p}{\partial x}\right|_{x=X_e}=0,\ \left.\frac{\partial p_p}{\partial y}\right|_{y=Y_e}=0 \quad (32)$$

$$\left.\frac{\partial p_p}{\partial z}\right|_{z=+h/2}=0,\ \left.\frac{\partial p_p}{\partial z}\right|_{z=-h/2}=0 \quad (33)$$

where h is the height of the shale reservoir, m; X_e, Y_e represent the value of maximum outer boundary in the x and y direction, respectively, m.

The SRV calculation model

In order to facilitate the simulation analysis, the stimulated reservoir volume is expressed with the volume of rock breaking. The simulation area is divided into grids, and let us say that the number of broken grids is n_s and the volume of grid destruction is V_{stb}, then SRV is the sum of all the damaged mesh; Fig. 5 is one-half of the three-dimensional SRV schematic:

$$SRV=\sum_{i}^{n_s}V_{stb}\left(i\right) \quad (34)$$

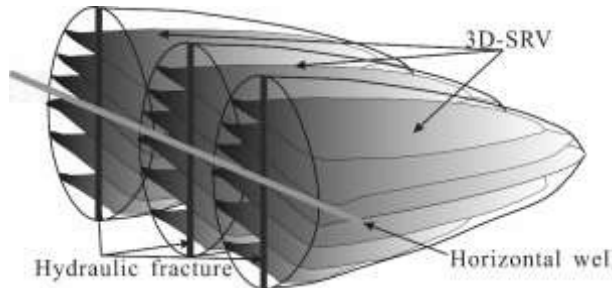

Fig. 5. The 3D SRV schematic diagram.

The calculation workflow

Based on elastic mechanics, seepage flow mechanics, the three-dimensional rock failure criteria, and material conservation principle, the model can be calculated. The calculation process of the model is shown in Fig. 6. The detailed calculation process is as follows:

1. Input basic geological parameters (initial reservoir permeability, initial reservoir pressure, cluster spacing, etc.) and construction parameters (pumping rate, pumping time, etc.).

2. Based on the fracture extension model and the material conservation equation, the fluid pressure distribution in the fracture, the length and width of fracture, and the fluid filtration loss through the fracture surface are obtained.

3. The distribution of fluid pressure in the crack, the length of the crack, and the height of the crack are used as the boundary of the finite element method module (FEMM) on the stress field of the reservoir, and the distribution of the geological stress after the interference can be obtained. Based on the change of ground stress, the normal stress and shear stress on the three-dimensional rock fracture surface can be obtained.

4. Then, the amount of fluid filtration is used as the source term in the boundary of fluid diffusion equation; the fracture fluid pressure is used as high pressure boundary; and the pore pressure distribution in the reservoir at any time can be obtained by the finite difference method module (FDMM). By substituting the pore pressure into the three-dimensional natural fracture damage criterion, it is possible to judge whether a tenor or shear failure on the natural fracture surfaces has been induced.

5. Finally, elements of the tensile and shear failure are integrated, and the volume of the transformed reservoir can be obtained.

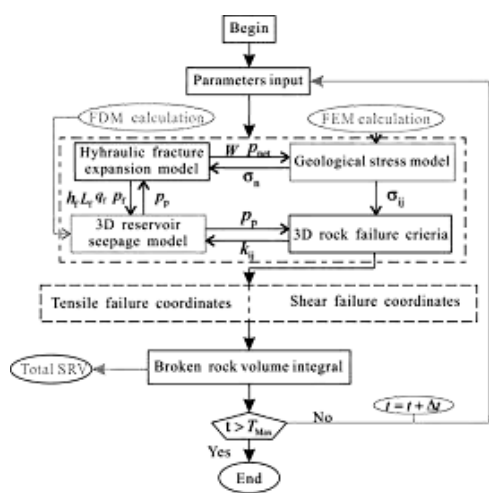

Fig. 6. The coupling program calculates the route.

CASE STUDIES

The basic parameters

The region of SRV in the actual shale reservoir is a near-symmetrical space shape. In order to reduce the computation and save the computation time, in this case only one-half of the whole model is taken. As shown in Fig. 1a, we chose a section of horizontal well fracturing as an example. The length, width, and height of the area are 500m, 200m, and 100m, respectively. The establishment of the global coordinate system is also shown in Fig.1b. In order to improve the calculation speed, the partition of the reservoir grid is divided by unequal spacing, and the grid encryption is carried out near the hydraulic crack and injection point of the water, as shown in Fig.1b. The number of total grids in the model is 56170. The basic parameters of the geological parameters and operation measures of the target reservoir are shown in Table 1.

Table 1. Construction and reservoir parameters in the model.

Parameters	Value	Units	Source
Pumping rate, Q_{inje}	15	m^3/min	Sun (2016)
Fluid viscosity,	10	mPa.s	Sun (2016)
Total injection volume, V_T	1500	m^3	Sun (2016)
Cluster spacing	30	m	Sun (2016)
Number of clusters	3	-	Sun (2016)
The size of the reservoir, (height*width*length)	100×200×500	m	Sun (2016)
Initial reservoir pressure, P_i	30	MPa	Ren et al. (2017)
Initial reservoir permeability, K_i (i=x,y,z)	0.0001	mD	Hu et al. (2016)
Reservoir porosity,	0.041	-	Hu et al. (2016)
Natural fracture spacing, S_f	0.4	m	Nassir et al. (2014)
Rock compressibility, C_r	4×10^{-3}	MPa^{-1}	Hu et al. (2016)
Fluid compressibility, C_l	8×10^{-4}	MPa^{-1}	Sun (2016)
Initial fluid volume factor, B_0	1.02	-	Sun (2016)
Natural fracture approaching angle,	45	°	Ren et al. (2017)
Natural fracture dip angle,	79	°	Ren et al. (2017)
Basic friction angle,	30	°C	Sun (2016)
Cohesive force,	0.5	MPa	Nassir et al. (2014)
Shear dilation angle,	3	°C	Hossain et al. (2002)
Shear stiffness, K_s	10000	MPa/m	Hossain et al. (2002)
Normal stiffness, K_n	20000	MPa/m	Guo and Liu (2014)
Vertical principal stress,	55	MPa	Ren et al. (2017)
Maximum horizontal principal stress,	50	MPa	Sun (2016)
Minimum horizontal principal stress,	45	MPa	Sun (2016)

DISCUSSIONS

The effect of stress interference

Based on the coupled FEMM of fluid pressure in the hydraulic fracture and reservoir geo-stress, the distribution of geo-stress induced after 30min of fracturing is shown in Fig.7, combined with the geological parameters in table 1. Fig. 7a, Fig. 7b, Fig. 7c, and Fig. 7d, respectively, represent that the stress induced in the reservoir is zero before fracturing, the induced stress distribution in the maximum horizontal principal stress direction after fracturing, the

induced stress distribution in the minimum horizontal principal stress direction, and the induced shear stress. It can be seen from Fig. 7 that the geological stress in the reservoir is greatly changed due to the fluid pressure in the hydraulic fracture, and the increase of the minimum principal stress and the maximum principal stress in the reservoir near the crack is greater. Considering the induced stress, the distribution of shear failure and tensile failure areas at 30 minutes after fracturing is obtained. As shown in Fig. 8, the area of shear failure areas in both horizontal and vertical sections is larger than the tensile failure areas.

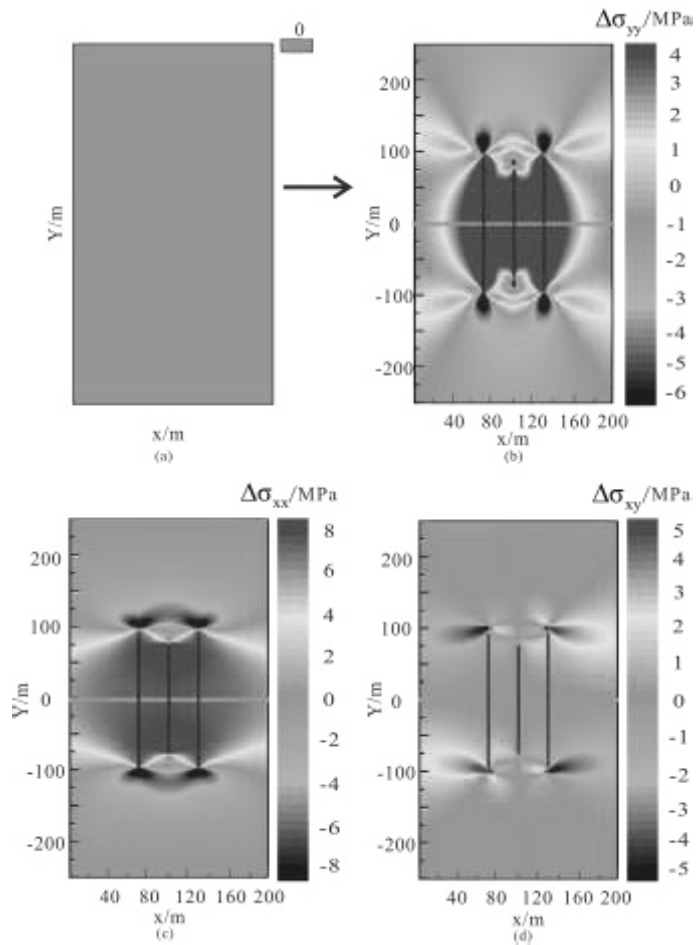

Fig. 7. The distribution of induced stress in the process of fracturing.

Based on the basic parameters in Table 1, we have obtained the relationships between tensile failure volume, shear failure volume, and time with the induced stress and without the induced stress, as shown in Fig. 9a. Meanwhile, the relationship between SRV and injection time can also be obtained, as shown in Fig. 9b. In Fig. 9a, compared with the case without considering the induced stress, the tensile failure volume is smaller when the induced stress is taken into account. But the shear failure volume is much larger considering the induced stress. Taken together, it can be seen from Fig. 9 that the SRV considering stress interference is larger than that without stress interference, but it is less than two-dimensional SRV with stress interference (Hu, 2017). According to formulae (19) and (20), when the principal stress increases, the normal stress and shear stress on the natural fracture surface will also increase. Compared to the case where stress interference is not considered, the increase in the normal stress will increase the difficulty of the tensile failure of natural fractures. But the increase of shear stress has the advantage of natural fracture slip and shear failure. And in a two-dimensional model, the height of SRV is equal to the height of the reservoir. However, in the

three-dimensional model, pore pressure dissipates in the vertical direction, and the height of SRV will be a variable value, not equal to the height of reservoir, especially in the early stage of fracturing and the edge of SRV. This results in the difference between two- and three-dimensional models. In Fig. 9, TF and SF denote tensile failure and shear failure, respectively.

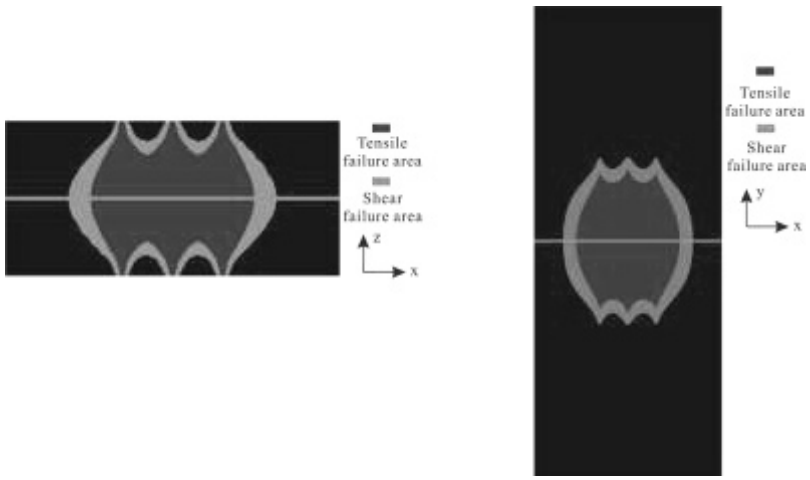

Fig. 8. Section profile of tensile failure and shear failure area in 30 minutes of fracturing.

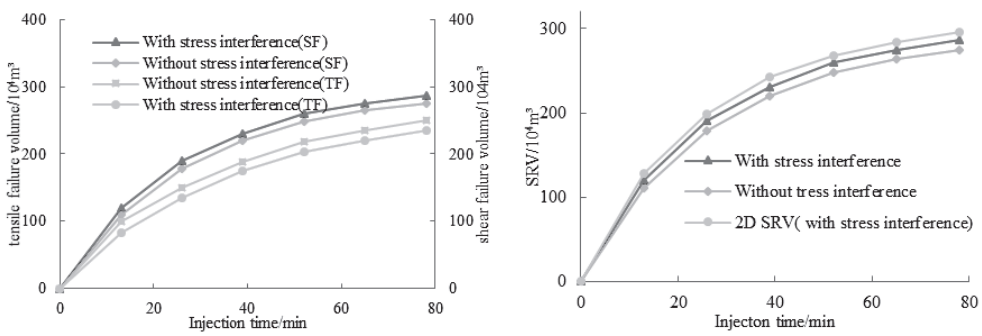

(a) (b)

Fig. 9. Effect of induced stress on SRV.

Three-dimensional SRV extension process

Based on the FEMM and the FDMM, plugging in the basic parameters in Tab.1, the stimulated reservoir volume coupled geological stress has been calculated. In order to verify the correctness of the simulation results, we obtained the field micro-seismic data for comparison, as shown in Fig.10. As you can see from Fig. 10, the simulated SRV region reflected by the increase of permeability is the same as the fracture network area reflected by micro-seismic cloud data. Therefore, the results of this model can be recognized.

The initial permeability of the reservoir is shown in Fig. 11a, which is one-quarter of the fracturing stimulated area along the x-y plane and the horizontal well. In order to fully display the three-dimensional SRV and permeability distribution, after the fracturing 25 minutes the SRV in height direction and permeability, respectively, are shown in Fig. 11b and Fig. 11c. These two diagrams are a quarter of the area, which is cut along the z - y plane and the middle perforating. As can be seen from Fig. 11a, the permeability of the shale reservoir matrix before fracturing is very low, only 0.0001mD. From Fig. 11b and Fig. 11c it can be seen that the shape of the permeability distribution and the SRV

are approaching semicircle after transforming. Meanwhile, the increased permeability is highest near the injection point and reduced along the radial direction gradually. By comparing with the permeability of the unmodified area, the permeability of the modified area is far greater than that of the unmodified zone.

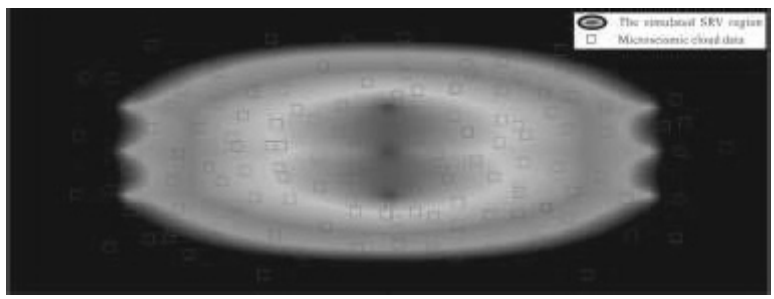

Fig. 10. The micro-seismic data of the x-y center plane is compared with the improvement permeability after fracturing.

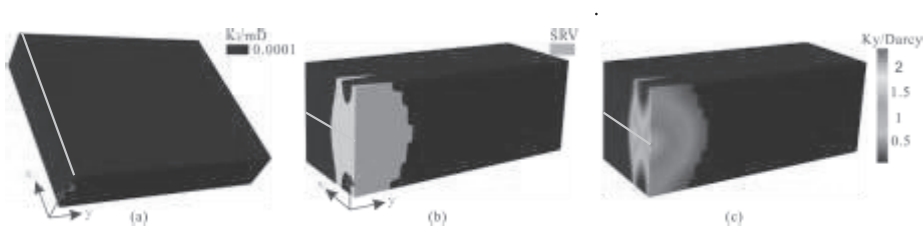

Fig. 11. Initial state and height direction result graph.

In order to fully reflect the three-dimensional change process of SRV during the fracturing process, the SRV maps of the 10 min, 40 min, and 100 min are shown in Fig. 12a, Fig. 12b, and Fig. 12c. At the same time, the relationship between SRV and injection time under the different approach angle (10°-50°) conditions is given, as shown in Fig. 13. It can be seen from Fig. 12 that the overall transformation volume is increasing with the increase of time. And the increase velocity of SRV along the y-axis (fracture expansion direction) is greater than that along the x-axis, so the overall length of the SRV is greater than its width after work. In this case, the SRV length is about 350 m, width 150 m or so. Since the shale reservoir has basically no influence on cover layer and the barrier layer, the SRV extends faster in the height direction. At the time of 35min, the shale reservoir of 100m thickness has been completely transformed. As can be seen from Fig. 13, with the increase of injection time, SRV increases under different approximation angle conditions. But as the approximation angle increases, the SRV decreases.

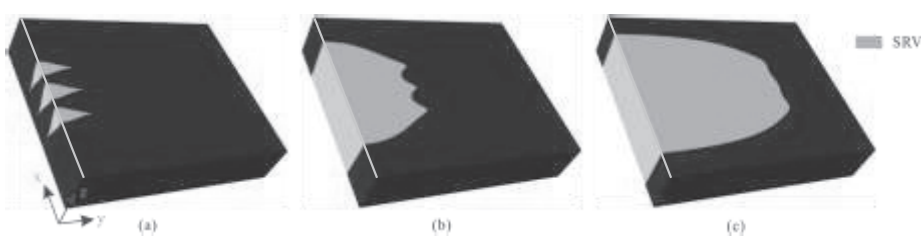

Fig. 12. The SRV 3D expansion process.

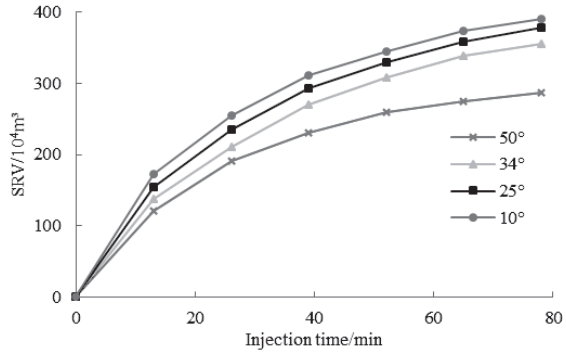

Fig. 13. The relationship between SRV and injection time at different dip angles.

The key effect of volume fracturing on shale gas productivity is that the low permeability of the original reservoir is increased. Therefore, the improvement of permeability after fracturing is the key index to characterize the stimulated volume. Fig. 14 is the distribution of reservoir permeability after fracturing. When the natural fractures are opened by the fluid pressure in the natural fractures, the permeability of reservoir has been greatly improved. In this case, the spatial distribution of natural fractures tends to be in the y direction, and the Ky tensor obtained by the coordinate system is the largest. In Fig. 14, the stimulated permeability has Ky>Kx>Kz, while the values of Kxy, Kyz, and Kxz are relatively close. Because of the spatial distribution of natural fractures and the size of principal stress, the value of Kz is the smallest.

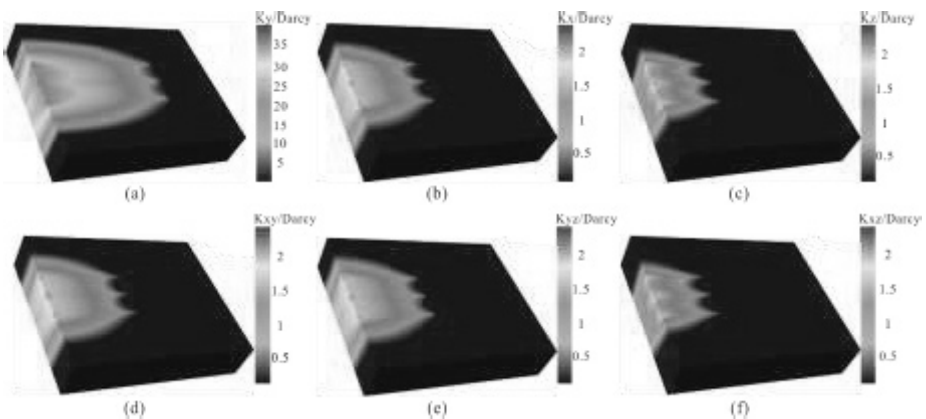

Fig. 14. Reservoir permeability distribution after hydraulic fracturing.

The effect of injection fluid volume

Fig. 15c represents the effect of the total injection fluid volume on the SRV volume in the same condition as other parameters (Dip angle is 79° and approaching angle is 35°). Fig. 15c represents that the total volume of SRV also increases with the injection fluid volume increasing, indicating that the injection fluid volume is one of the important factors affecting SRV size. As the volume of injected fluid increases in Fig. 15a, the length and width of SRV also increase. And with the increase in the injected fluid volume, the height of the SRV increases first and then maintains 100 m, as shown in Fig. 15b. This is because when the injected fluid volume reaches a certain amount, the 100 m thickness reservoir is completely penetrated by hydraulic fracture, and the reservoir near the hydraulic crack is completely transformed. Fig. 16a and Fig. 16b represent the permeability distribution cloud map of the transformed area under the condition that the injection fluid volume is 550m³ and 1100m³, respectively, and its shape is similar to the shape of SRV. Comparing these two figures, we can find that the length and width of the reconstructed area after

the injected volume of 1100m³ are greater than the length and width of the modified volume of the injected volume of 550m³. Therefore, the injection fluid volume is one of the important factors affecting SRV size.

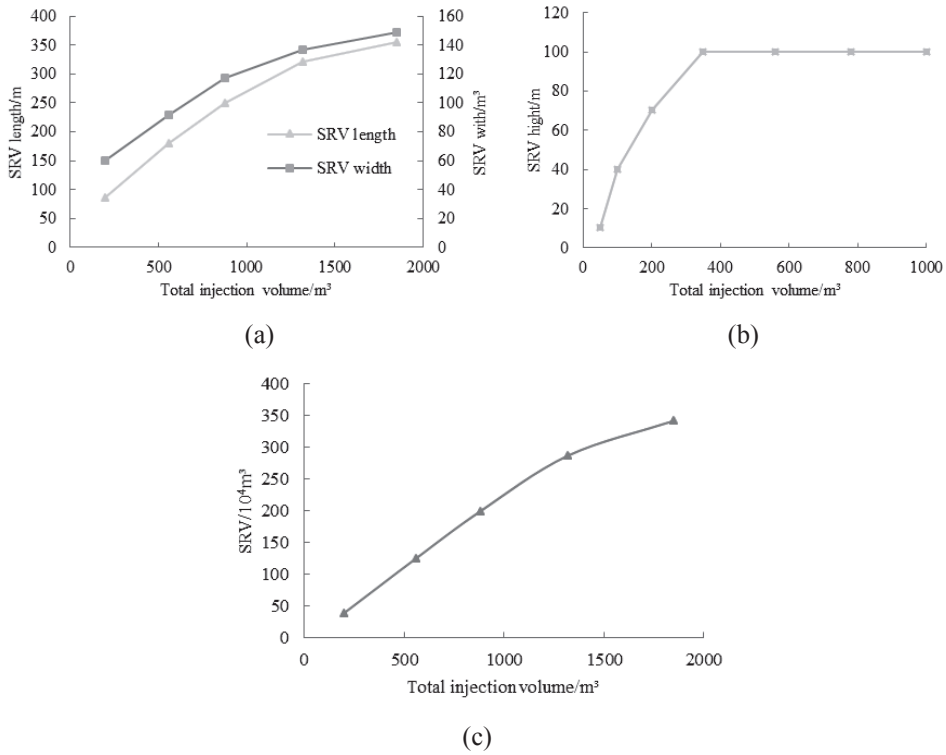

Fig. 15. Influence of injected fluid volume on SRV size.

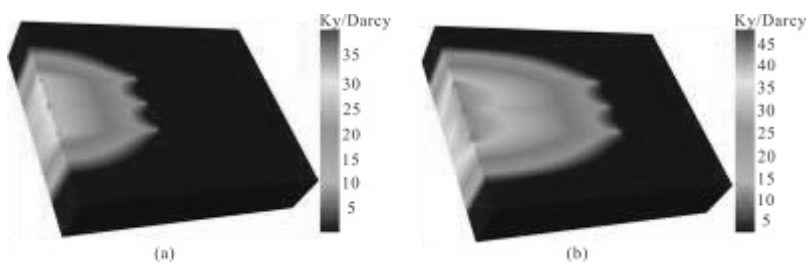

Fig. 16. The distribution of permeability under different injection total fluid volume.

The influence of natural fracture space distribution

Fig. 17b represents the influence of natural fracture approaching angle on SRV under the condition of the horizontal principal stress difference (5MPa) and the total injection fluid (1500m³). It can be seen that the SRV decreases with the increase of the approaching angle of the natural fractures, and the SRV decreases rapidly when the approaching angle is close to 35°. The effect of natural fracture approaching angle on the length and width of SRV is shown in Fig. 17a. As the approaching angle increases, the length of SRV increases gradually, and the width decreases gradually. When the approaching angle is close to 35°, rate of change has accelerated. Fig. 18b also shows the influence of natural fracture dip on SRV under the condition of 5MPa with 1500m³ of injected fluid and horizontal principal stress difference. With the increase of natural fracture dip angle, the SRV will increase, and the rate of change is reduced. In Fig. 18a the length of SRV gradually increases with the increase of the dip angle of natural fractures, and the width

decreases gradually. When the angle is less than 40°, length and width of SRV change quickly, and after more than 40° change slowly. From Fig.15b, it can be seen that when the fluid volume is close to 400m³, the reservoir of 100m thickness has been penetrated by the transformed region. In this case, the total volume of the injected fluid is 1000m³, and the height of SRV is already 100m, so the influence of approaching angle and dip angle on SRV is mainly reflected in length and width. When the natural fracture approaching angle is 25° and 55°, respectively, the distribution of the stimulated permeability is shown in Fig. 19. It can be seen that, in the case of main stress $\sigma_v > \sigma_H > \sigma_h$, the smaller the approaching angle of the natural crack is and the larger the dip angle is, the more easily the shale reservoir is transformed. Therefore, the approaching angle and dip angle of natural fractures are the important factors for SRV.

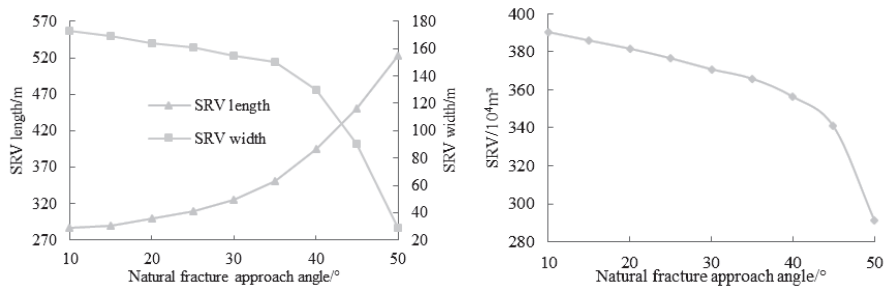

(a) (b)

Fig. 17. Influence of natural fracture approaching angle on SRV.

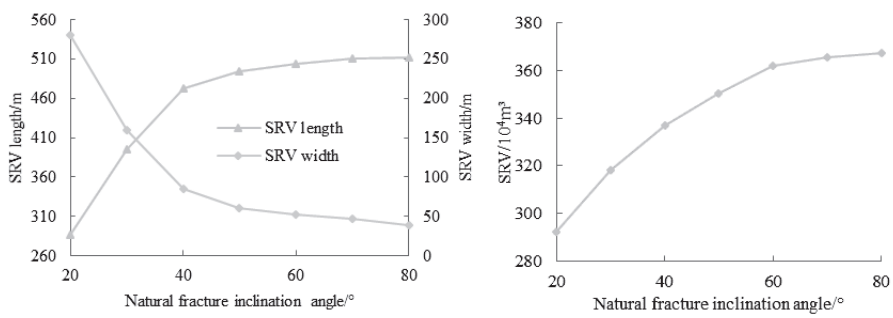

(a) (b)

Fig. 18. Influence of natural fracture dip angle on SRV.

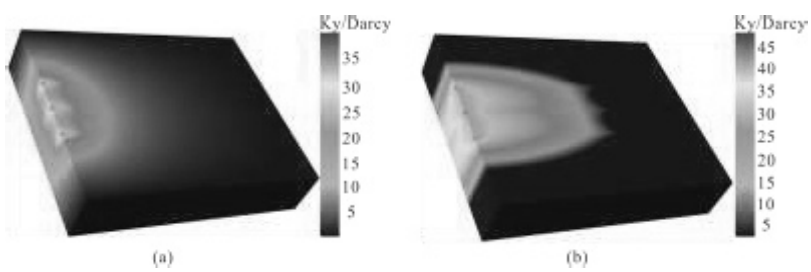

Fig. 19. Influence of natural fracture approaching angle on permeability distribution.

The effect of horizontal principal stress difference

Fig. 20b represents the effect of horizontal principal stress difference on SRV in the case of the injection fluid volume of 1500 m³, the approaching angle of 35°, and the dip angle of 79°. The SRV decreases with the increase of horizontal principal stress difference. Fig. 20a indicates the effect of horizontal principal stress difference on the length and width of SRV. The length of SRV increases with the increase of horizontal principal stress, while the width of SRV decreases with the increase of horizontal principal stress. Since the SRV height has reached 100m and remains unchanged, there is no further discussion. Fig.21 a is the permeability distribution cloud map of the improved shale reservoir under the stress difference of 5MPa. Fig. 21b is a distribution cloud map obtained under the condition of stress difference 2MPa. Comparing these two clouds, it can be proved that the higher the horizontal principal stress difference is, the longer the SRV length is, and the smaller the width is, the smaller the SRV is. Therefore, the low horizontal principal stress difference is conducive to the transformation of shale reservoir. So the horizontal principal stress difference is another key factor affecting SRV.

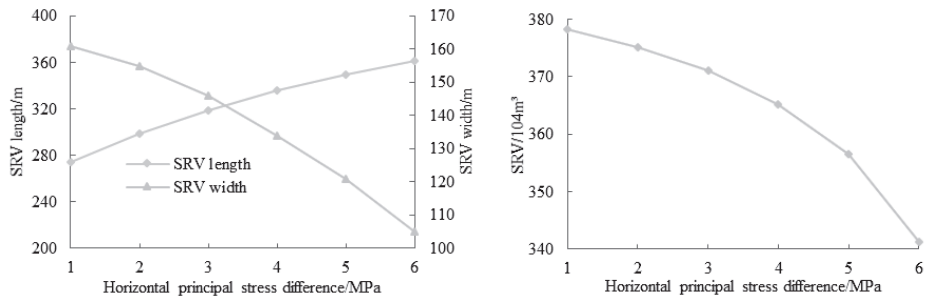

Fig. 20. Influence of horizontal principal stress difference on SRV.

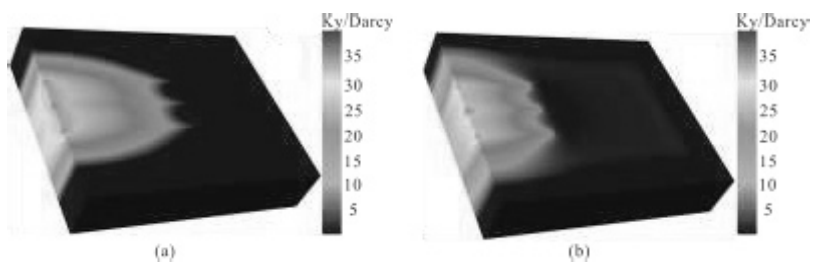

Fig. 21. Influence of horizontal principal stress difference on transformation permeability.

CONCLUSIONS

Based on stress interference of FEMM, the three-dimensional rock failure criterion, the total permeability tensor, and the 3D fluid diffusion equation of FDMM, a mathematical model for predicting the SRV by hydraulic fracturing is established. The change process of the SRV size and the reservoir permeability dynamically have been simulated, and the influence factors of SRV have been analyzed, including injection volume, natural fracture distribution, and horizontal principal stress. Finally, the following conclusions are drawn:

1) Compared with no consideration of stress interference, the difficulty of tensile failure on natural fractures near the hydraulic fracture increases with the influence of fluid pressure in hydraulic fractures, but shear failure is more likely to occur. The total SRV will be larger considering the induced stress.

2) When hydraulic fracturing technology is used in the shale gas reservoir to improve the production, the tensile or shear failure of natural fractures near the hydraulic fracture occurs firstly. As the fluid is injected, the damage area is

gradually extended. The direct result of failure is that the permeability of the shale reservoir with low permeability is greatly improved, which creates conditions for later production. Therefore, the fundamental expression of SRV is that the permeability of the stimulated area is greatly increased.

3) During the fracturing process, the total volume of injected fluid has an important influence on the size of SRV. The larger the injection volume is, the larger the length and width of SRV and the SRV size are. Meanwhile, the magnitude of the horizontal principal stress difference has a great influence on SRV. The larger the horizontal principal stress difference is, the smaller the SRV size and its width are, but the larger the length is. Therefore, the larger the total injection fluid volume is and the smaller the horizontal principal stress difference of the target layer is, the more favorable it is to increase the SRV size.

4) The approaching angle and dip angle of natural fractures have a critical influence on the size of SRV. Under the condition that the principal stress is $\sigma_v > \sigma_H > \sigma_h$, the SRV and its width decrease and its length increases when the approaching angle increases. At the same time, when the dip angle increases, the SRV and length of SRV increase, while its width decreases. Therefore, under the condition of this principal stress, the smaller the approaching angle is, the more favorable it is to increase the volume of SRV.

ACKNOWLEDGMENT

The work presented in this paper was supported by the major program of China National Petroleum Corporation (2016E-01) and National Science and Technology Major Special Project-Fu Ling shale gas development demonstration project (2016ZX05060).

REFERENCES

Cipolla, C.L. 2009. Modeling production and evaluating fracture performance in unconventional gas reservoirs. J. Pet. Technol., 9(61):84–90

Fanchi, J.R. 2008. Directional permeability. SPE Reserv. Eval. Eng., 11(03):565–568

Fredd, C.N., McConnell, S.B., Boney, C.L. & England, K.W. 2001. Experimental study of fracture conductivity for water-fracturing and conventional fracturing applications. SPE J., 6(03):288–298

Ge, J. & Ghassemi, A. 2012. Stimulated reservoir volume by hydraulic fracturing in naturally fractured shale gas reservoirs. In: 46th US rock mechanics/geomechanics symposium. American RockMechanics Association, 24–27 June, Chicago

Ghassemi, A., Zhou, X.X. & Rawal, C. 2013. A three-dimensional poroelastic analysis of rock failure around a hydraulic fracture. J. Pet. Sci. Eng., 108:118–127

Guo, J. & Liu, Y. 2014a. A comprehensive model for simulating fracturing fluid leakoff in natural fractures. J. Nat. Gas Sci. Eng., 21:977–985

Guo, J. & Liu, Y. 2014b. Opening of natural fracture and its effect on leakoff behavior in fractured gas reservoirs. J. Nat. Gas Sci. Eng., 18:324–328

Hossain, M.M., Rahman, M.K. & Rahman, S.S. 2002. A shear dilation stimulation model for production enhancement from naturally fractured reservoirs. SPE J., 7(02):183–195

Hu, Y.Q., Li, Z.Q., Zhao, J.Z., Ren, L. & Wang, D. 2016. Optimization of hydraulic fracture-network parameters based on production simulation in shale gas reservoirs. J. Eng. Res., 4(04):159–180

Maulianda, B.T., Hareland, G. & Chen, S.2014. Geomechanical consideration in stimulated reservoir volume dimension models prediction during multi-stage hydraulic fractures in horizontal Wells–Glauconite tight formation in Hoadley field. In: 48th US rock mechanics/ geomechanics symposium. American Rock Mechanics Association

Mayerhofer, M.J., Lolon, E.P., Warpinski, N.R. & Walser, D.W. 2010. What is stimulated reservoir volume (SRV)? SPE Prod. Oper., 15(4):473–485

Nassir, M., Settari, A. & Wan, R.G. 2012. Prediction and optimization of fracturing in tight gas and shale using a coupled geomechanical model of combined tensile and shear fracturing. In: Paper SPE-152200-MS presented at the SPE hydraulic

fracturing technology conference, 6–8 February, The Woodlands

Nassir, M., Settari, A. & Wan, R.G. 2014. Prediction of stimulated reservoir volume and optimization of fracturing in tight gas and shale with a fully elasto-plastic coupled geomechanical model. SPE J., 19(05):771–785

Palmer, I., Cameron, J. & Moschovidis, Z. 2009. Natural fractures influence shear stimulation direction. Oil Gas J., 107(12):37–43

Palmer, I.D., Moschovidis, Z.A. & Cameron, J.R. 2007. Modeling shear failure and stimulation of the Barnett shale after hydraulic fracturing. In: Paper SPE-106113-MS presented at the hydraulic fracturing technology conference, 29–31 January, College Station

Palmer, I.D., Moschovidis, Z.A. & Schaefer, A. 2013. Microseismic clouds: modeling and implications. SPE Prod. Oper., 28(02):181–190

Ren, L., Lin, R., Zhao, J. & Wu, L. 2017. Cluster spacing optimal design for staged fracturing in horizontal shale gas wells based on optimal SRV. Natural Gas Industry, 47(4): 69-79

Ren, L., Lin, R., Zhao, J. Rasouli, V., Zhao, J. & Yang, H. 2017. Stimulated reservoir volume estimation for shale gas fracturing: Mechanism and modeling approaching. J. Pet. Sci. Eng., 166:290-304

Ren, L., Su, Y., Zhan, S., Hao, Y., Meng, F. & Sheng G. 2016. Modeling and simulation of complex fracture network propagation with SRV fracturing in unconventional shale reservoirs. J. Nat. Gas Sci. Eng., 28:132–141

Ren, L., Lin, R., Zhao, J, Yang, K., Hu, Y. & Wang, X. 2015. Simultaneous hydraulic fracturing of ultra-low permeability sandstone reservoirs in China: Mechanism and its field test. Journal of Central South University, 22(4):1427-1436.

Shahid, A.S.A., Wassing, B.B.T., Fokker, P.A. & Verga, F. 2015. Natural-fracture reactivation in shale gas reservoir and resulting microseismicity. J. Can. Pet. Technol., 54(06):450–459

Sun, R.Z. 2016. The research on the calculation method of stimulated reservoir volume for shale gas reservoir in Fuling area of China. Master Degree Thesis, Southwest Petroleum University

Wang, Y., Li, X., Zhou, R.Q. & Tang, C. 2016. Numerical evaluation of the shear stimulation effect in naturally fractured formations. Sci. China Earth Sci., 59(2):371–383

Warpinski, N.R. & Teufel, L.W. 1987. Influence of geologic discontinuities on hydraulic fracture propagation. JPT, 39(2):209-220.

Warpinski, N.R., Wolhart, S.L. & Wright, C.A. 2001. Analysis and prediction of microseismicity induced by hydraulic fracturing. In: Paper SPE 71649-MS presented at the SPE annual technical conference and exhibition, 30 September–3 October, New Orleans

Weng, X., Kresse, O., Cohen, C., Wu, R. & Gu, H. 2011. Modeling of hydraulic fracture-network propagation in a naturally fractured formation. SPE Prod. Oper., 26(04):368–380

Xu, W., Thiercelin, M., Ganguly, U., Weng, X. & Gu, H. 2010. Wiremesh: a novel shale fracturing simulator. In: Paper SPE 132218 presented at CPS/SPE international oil and gas conference and exhibition, 8–10 June, Beijing

Xu, W., Thiercelin, M.J. & Walton, I.C. 2009. Characterization of hydraulically-induced shale fracture network using an analytical/semi-analytical model. In: Paper SPE 124697-MS presented at the SPE annual technical conference and exhibition, 4–7 October, New Orleans

Yu, G. & Aguilera, R. 2012. 3D analytical modeling of hydraulic fracturing stimulated reservoir volume. In: Paper SPE-153468 presented at SPE Latin America and Caribbean petroleum engineering conference, 16–18 April, Mexico City

Hu, Y., Li, Z., Zhao, J., Tao, Z. & Gao, P. 2017. Prediction and analysis of the stimulated reservoir volume for shale gas reservoirs based on rock failure mechanism. Environmental Earth Sciences, 15(76):546

Zhang, J., Kamenov, A. & Zhu, D. 2013. Laboratory measurement of hydraulic fracture conductivities in the Barnett shale. In: Paper IPTC-16444-MS presented at the international petroleum technology conference, 26–28 March, Beijing

Zhou, L. & Hou, M.Z. 2013. A new numerical 3D-model for simulation of hydraulic fracturing in consideration of hydro-mechanical coupling effects. Int. J. Rock Mech. Min. Sci., 60:370–380.

Zhou, L., Hou, M.Z., Gou, Y. & Li, M. 2014. Numerical investigation of a low-efficient hydraulic fracturing operation in a tight

gas reservoir in the North German Basin. Journal of Petroleum Science and Engineering, 120:119-129

Zimmerman, R.W., Kumar, S. & Bodvarsson, G.S. 1991. Lubrication theory analysis of the permeability of rough-walled fractures. Int. J. Rock Mech. Min. Sci., 1991, 28, 325–331

Zou, Y., Zhang, S., Ma, X. Zhou, T. & Zeng, B. 2016. Numerical investigation of hydraulic fracture network propagation in naturally fractured shale formations. J. Struct. Geol., 84:1–13

Submitted: 25/06/2018
Revised: 10/08/2018
Accepted: 16/08/2018

نموذج عددي لمحاكاة الشبكة التي يسببها الكسر الهيدروليكي لخزان الغاز الصخري الثلاثي الابعاد مع تداخل الإجهاد الجغرافي

تشيانغ وانغ، يونغكوان هو، جينتشو جاو و رين ايان
مختبر الدولة الرئيسي لاحتياطيات النفط والغاز الجيولوجي والاستغلال، جامعه جنوب غرب النفط، تشنغدو 610500، الصين

الخلاصة

في الثنائي الابعاد محاكاة نموذج حجم الخزان ، يتم تحديد موقف الكسور الطبيعية فقط من زاوية تقترب ، وانها ليست سوي اللازمة للنظر في تاثير الإجهاد الرئيسي الأفقي في معيار الفشل. في الخزان الزيتي ثلاثي الابعاد ، يجب تحديد موقع الكسر الطبيعي بزاوية الانحدار وزاوية الاقتراب مع النظر في تاثير الضغط الرئيسي الراسي والأفقي في معيار الفشل. الاضافه إلى ذلك ، فان فتح العديد من الشقوق الهيدروليكية في نفس الوقت سيؤدي إلى تغيير الإجهاد الجيولوجي ، مما يتسبب في تغير ظروف الكسر الطبيعي وفشل القص من جانب الخصلة المستحثة. من أجل تحليل جيل من ثلاثه الابعاد شبكه الكسر ، وهذه الورقة يؤسس نموذجا رياضيا علي أساس ميكانيكا مرنه ، وثلاثه الابعاد الصخرة المعيار الفشل ، والقدرة علي الاختراق الكامل والمعادلة الحفاظ علي المواد. أولا ، يتم إنشاء نموذج أسلوب العنصر المحدود من الإجهاد الجيولوجي الناجمة عن كسر علي أساس نموذج انتشار الكراك ، والفرق المحدودة طريقه الوحدة القائمة علي ثلاثه الابعاد السوائل التحكم في انتشار المعادلة والنفاذيه الكاملة ويستخدم تيسور لحل توزيع الضغط الخازن. ثم يتم استخدام معايير الشد والقص الصخري ثلاثية الابعاد لتحديد ما إذا كان قد تم اتلاف إيه وحدات شبكه. وبمجرد حدوث الشبكة في اي شكل من اشكال الفشل في الصخور ، فان نفاذيه وحده الشبكة المناظرة ستتغير أيضا بسبب تغير فتحه الكسر الطبيعي. وأخيرا ، فان حجم المكمن المحفز تمثله المنطقة التي تزداد فيها النفاذيه. وتعرض هذه الورقة تحليل حساسية العوامل المتعددة بعد استخدام البيانات السيزميه الدقيقة للتحقق من النموذج العددي ، بما في ذلك تاثير حجم السوائل المحقونة ، والكسر الطبيعي الذي يقترب من الزاوية ، وزاوية الانحدار ، والإجهاد الرئيسي الأفقي الفرق علي حجم محاكاة حجم الخزان (الشكل ، والحجم ، والحدود العرض ، والطول ، وآخرون). وتظهر النتائج انه بالمقارنة بدون الإجهاد المستحث ، ينخفض حجم فشل الشد ، ويزيد حجم فشل القص ، ويزيد إجمالي حجم الخزان المحاكي بسبب الإجهاد المستحث. وعندما يكون الإجهاد الرئيسي الراسي في الإجهاد الرئيسي الثلاثة هو الحد الأقصى ، يزيد طول حجم الخزان المحاكي مع زيادات الكسور الطبيعية التي تقترب من الزاوية ، وزاوية الانحدار ، وفرق الإجهاد الرئيسي الأفقي ، وعرضها الذي ينخفض. ويزيد عرضها وطولها في نفس الوقت فقط مع زيادة حجم السوائل المحقونة ؛ ويزيد حجم الخزان المحاكي مع زيادة حجم سوائل الحقن وانخفاض الكسر الطبيعي ، ولكن مع الزيادة في الكسر الطبيعي الذي يقترب من الزاوية والاختلاف الأفقي في الإجهاد الرئيسي.